Proceedings of the ASME 2019
Internal Combustion Engine Division Fall Technical Conference
ICEF2019
October 20-23, 2019, Chicago, IL, USA

ICEF2019-7130

INVESTIGATION INTO REACTIVITY SEPARATION BETWEEN DIRECT INJECTED AND PREMIXED FUELS IN RCCI COMBUSTION MODE

Ziming Yan[1], Brian Gainey, Deivanayagam Hariharan, Benjamin Lawler[2]
Stony Brook University
Stony Brook, NY

ABSTRACT

This experimental study focuses on the effects of the reactivity separation between the port injected fuel and the direct injection fuel, the amount of external-cooled exhaust gas recirculation (EGR), and the direct injection timing of the high reactivity fuel on Reactivity Controlled Compression Ignition (RCCI) combustion. The experiments were conducted on a light-duty, single-cylinder diesel engine with a production GM/Isuzu engine head and piston and a retrofitted port fuel injection system. The global charge-mass equivalence ratio, ϕ', was fixed at 0.32 throughout all of the experiments. To investigate the effects of the fuel reactivity separation, different Primary Reference Fuels (PRF) were port injected, with the PRF number varying from 50 to 90. To investigate the effects of EGR, an EGR range of 0 to 55% was used. To investigate the effects of the injection timing, an injection timing window of -65 to -45 degrees ATDC was chosen.

The results indicate that there are several tradeoffs. First, decreasing the port injected fuel reactivity (increasing the PRF number) delays combustion phasing, decreases the combustion efficiency by up to 9%, increases the gross indicated thermal efficiency up to 22%, enhances the combustion sensitivity to the direct injection timing, and slightly increases the UHC, CO, and NOx emissions. Second, increasing the EGR percentage delays combustion phasing, lowers the peak heat release rate, and lowers the NOx emissions. The combustion efficiency first increases and then decreases with EGR percentage for high reactivity fuels (low PRF number), but only decreases for low reactivity fuels. Finally, delaying the injection timing advances combustion phasing and increases the combustion efficiency, but decreases the gross indicated thermal efficiency and increases the NOx emissions. Across all of the experiments, delays in CA50 increase the gross indicated thermal efficiency and decrease the combustion efficiency, which represents an inherent tradeoff for RCCI combustion on a light-duty engine.

Keywords: Internal Combustion Engines; RCCI; Fuel reactivity separation; Diesel; Primary Reference Fuels; EGR.

NOMENCLATURE

aTDC	after top dead center
CAD	crank angle degree
CA50	crank angle of 50% mass fraction burned
CDC	conventional diesel combustion
CO	carbon monoxide
COV	coefficient of variation
DI	direct injected
DTBP	di-tert-butyl peroxide
EGR	external-cooled exhaust gas recirculation
EVO	exhaust valve open
GHRR	gross heat release rate
HCCI	homogeneous charge compression ignition
$IMEP_n$	net indicated effective mean pressure
IVO	intake valve open
LTC	low-temperature combustion
LTHR	low temperature heat release
MFB	mass fraction burned
NHRR	net heat release rate
NO_x	nitrogen oxides
OEM	original equipment manufacturer
PCCI	premixed charge compression ignition
PFI	port fuel injected
PM	particulate matter
PPRR	peak pressure rise rate
PRF	primary reference fuels
RCCI	reactivity-controlled compression ignition
SOI	start of injection
TSCI	thermally stratified compression ignition
ULSD	ultra-low sulfur diesel
UHC	unburned hydrocarbon

[1] Contact author: Yan.ziming@stonybrook.edu
[2] Contact author: Benjamin.lawler@stonybrook.edu

1. INTRODUCTION

The internal combustion engine has been the most reliable energy conversion device for transportation applications for more than 100 years. With the advancement of technology and the desire to increase energy efficiency, society's demands and government regulations on internal combustion engines continue to become more aggressive. Traditional combustion modes, like Spark Ignition (SI) and Conventional Diesel Combustion (CDC), will not be able to meet these requirements and regulations in the near future due to low thermal efficiencies and excessive soot/NOx emissions, respectively [1-6]. To address these shortcomings, several advanced combustion modes have been proposed including a variety of Low-Temperature Combustion (LTC) modes [7]. LTC focuses on maintaining the in-cylinder temperatures below the NO_x production threshold by keeping the global equivalence ratios low, which also yields high thermal efficiencies. Several advanced, LTC modes currently being investigated are Homogeneous Charge Compression Ignition (HCCI) [8-13], Premixed Charge Compression Ignition (PCCI) [14-16], Thermally Stratified Compression Ignition (TSCI) [17-18], and Dual-fuel Reactivity Controlled Compression Ignition (RCCI) [19-28]. Each of these strategies has advantages and drawbacks. For example, HCCI is known for its high efficiency and low NOx and PM emissions from lean, homogeneous operation, but also for its low combustion efficiency (i.e., high CO and UHC emissions) and lack of control over the start and rate heat release, which result in a narrow operational load range [29-31]. RCCI, despite facing a commercialization challenge due to the higher cost and complexity of its two distinct fuel systems, has good controllability and a large operating range, with HCCI-like efficiencies and emissions.

In RCCI, two different fuels with different autoigntion tendencies are used. As shown in *Figure 1*, a low reactivity fuel, such as gasoline, is injected into the intake manifold or port to create a homogeneous mixture of air and fuel which is inducted into the cylinder during the intake stroke. Separately, a high reactivity fuel, like diesel, is directly injected into the cylinder during the mid-to-late compression stroke. The timing of the direct injection event, the ratios of the high and low reactivity fuels, and the specific fuels used dictate the in-cylinder reactivity stratification, which is the key factor for controlling the combustion process in RCCI, including the combustion phasing (CA50) and the heat release rate (HRR). Previous experiments showed that RCCI is highly controllable by different injection strategies, such as experimental and computational works conducted by Splitter et al., which showed that different injection timings and the use of multiple direct injections can improve the emissions and efficiencies [19]. Further work conducted by DelVescovo extended the injection timing window and explored that a potential shift in combustion regime happened when retarding SOI from -140 degrees to -35 degrees aTDC [20]. Walker et al. investigated that low direct injection pressures with a production re-entrant piston resulted in comparable emissions, but slightly lower combustion efficiency [21].

A large quantity of research was conducted using gasoline as the low reactivity fuel [22-26]. Some research work conducted by Dempsey et al. investigated the effects of using a cetane improver to achieve "single-fuel RCCI". Gasoline (96 octane) was used as the port injected fuel and the same gasoline mixed with 2-ethylhexyl nitrate (2-EHN) was used as the direct injected fuel. With this method, RCCI could be enabled from a single fuel, with an additive tank that could be refilled at oil-change intervals. However, the EHN resulted in an increase of NOx emissions compared with gasoline-diesel RCCI, due to the fuel-bound NOx group in the EHN [27]. Experimental and computational works from Splitter et al. showed that the specific fuel combinations, such as gasoline-diesel, e85-diesel, and gasoline-gasoline+DTBP, played a strong role in the combustion characteristics that resulted from RCCI combustion [28].

All of these studies demonstrated that the key factor of RCCI is the in-cylinder reactivity gradient, which can be directly affected by the reactivity separation between the high and low reactivity fuels, along with the injection strategy and residual gas fraction. However, the effects of the reactivity of the port injected fuel, combined with the effects of EGR and injection timing, have not yet been explored systematically, which is the motivation for this study: to evaluate the effects of the reactivity separation between the high and low reactivity fuels, while also organizing the effects of injection timing and EGR on combustion on a light-duty compression ignition engine operating in RCCI. In order to investigate the effects of different reactivity separations in RCCI combustion, the "gasoline" in *Figure 1* was substituted with different primary reference fuel (PRF) blends, with PRF numbers ranging from 50 to 90, in increments of 10. Meanwhile, EGR was applied from 0% to 55% to understand the combined effects of EGR, injection timing, and reactivity separation on the combustion and emissions characteristics of RCCI.

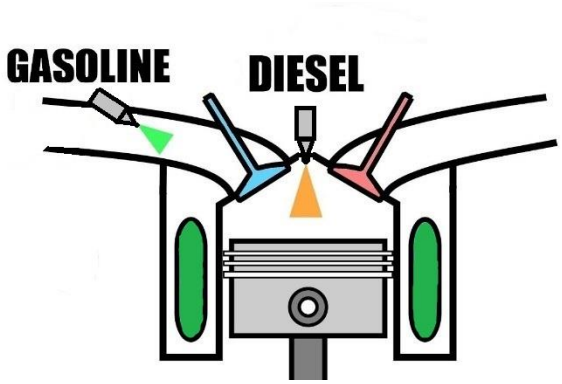

FIGURE 1: ILLUSTRATION OF RCCI COMBUSTION

2. EXPERIMENTAL SETUP

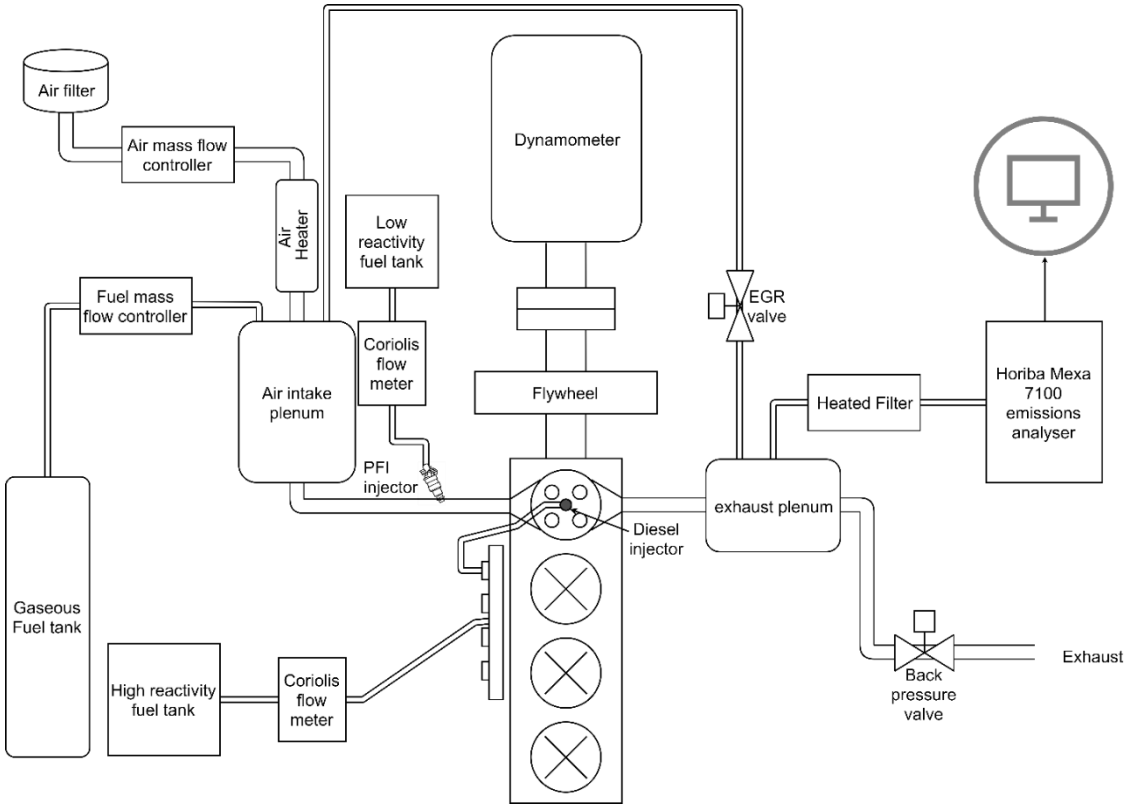

Figure 2: SCHEMATIC OF THE EXPERIMENTAL TEST CELL

2.1 Engine setup and measurements

A single-cylinder, light-duty compression ignition engine was used in this study. A schematic of the entire system is shown in ***Figure 2***. The production head had four cylinders, but only one was used. The engine head was from a production General Motors/Isuzu 4-cylinders, 1.7-liter diesel engine, and the first cylinder was mounted to a Ricardo Hydra single-cylinder engine block. The engine geometry and valve timings are listed in ***Table 1***. Although a previous study [32] showed that the combustion efficiency would be higher if a modified wide shallow bowl piston is used for RCCI, the original equipment manufacturer (OEM) diesel-style re-entrant bowl piston was used in this study. The piston geometry used is shown in ***Figure 3***, which shows a cut-plane of the cylinder**.**

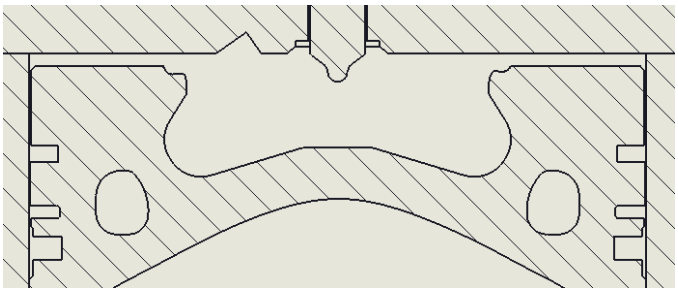

Figure 3: COMBUSTION CHAMBER AT TDC

Table 1: ENGINE PARAMETERS

Displacement [cc]	421.5
Bore x Stroke [mm]	79 x 86
Connecting Rod Length [mm]	160
Number of Valves	4
IVO [deg ATDC]	-366
IVC [deg ATDC]	-146
EVO [deg ATDC]	-122
EVC [deg ATDC]	-366
Compression Ratio	15.5

The intake air mass flow was controlled and monitored by an Alicat Scientific MCRW-1000 mass flow controller and meter. Before flowing into the intake plenum, the intake air passes through a 5 kW intake heater, which is triggered by a PID controller in a custom Labview program to control the intake temperature. The intake temperature is measured by a K-type thermocouple immediately before the intake port. On the exhaust side, a backpressure valve was used to control the exhaust pressure. The exhaust plenum is connected to the intake plenum by an external-cooled EGR line and the EGR line temperature is measured by a K-type thermocouple in the line. The EGR line is wrapped with heat tape which is also controlled by a PID

controller in the custom Labview program; the EGR flow is regulated by an electronically controlled valve. The percentage of EGR was calculated from the ratio of CO_2 in the intake to CO_2 in the exhaust, as measured by a Horiba MEXA 7100 D-EGR emissions analyzer.

In this study, PRFs are used as the low reactivity fuel, which are port fuel injected (PFI) into the intake manifold. The two PRFs, iso-octane and n-heptane, are blended together to create fuel surrogates whose PRF number were determined by the following equation:

$$PRF\# = \frac{mass_{iso-Octane}}{mass_{iso-Octane}+mass_{n-Heptane}} \quad (1)$$

Since the density and lower heating value of both PRFs are nearly identical, the PRF number can be calculated on a mass basis, volume basis, or energy basis, and the differences are negligible.

The high reactivity fuel is delivered by a Bosch, solenoid-style, 6-hole diesel injector using a high-pressure common rail. The common rail was pressurized by an electric motor-driven Bosch CP3 pump and maintained at 730 bar. The fuel flow for both the low and high reactivity fuels was measured by two Micro Motion Coriolis flow meters. The properties of the PFI and DI fuels are listed in *Table 2*.

The cylinder pressure was measured by a Kistler 6041A high-speed cylinder pressure transducer and was pegged to the intake pressure. The intake, exhaust, and diesel common rail pressure were measured by a Kistler 4011A, a Kistler 4049B, and a Kistler 4067E high-speed pressure transducer, respectively. All of the high-speed pressure measurements are triggered by a Kistler 2614C11 crank angle encoder coupled to a pulse-multiplier, whose final resolution is 0.1 degrees.

Heated and filtered exhaust gas was delivered to a Horiba MEXA-7100D-EGR emissions analyzer, which measures five types of exhaust emissions: unburned hydrocarbons (UHC), oxides of nitrogen (NO and NO_2, i.e., NOx), CO, CO_2 and O_2. In the emissions bench, UHC are measured with a flame ionization detector (FID), NOx are measured with a chemiluminescence detector (CLD), both CO and CO_2 are measured with a non-dispersive infrared detector (NDIR), and the oxygen is measured by a paramagnetic detector.

Table 2: FUEL PROPERTIES

Fuel	iso-Octane	n-Heptane	Diesel
Chemical Formula	C_8H_{18}	C_7H_{16}	-
H/C Ratio	2.25	2.286	1.777
O/C Ratio	0	0	0
Sulfur [ppm]	0	0	10
Q_{LHV} [kJ/kg]	44427	44566	42061
RON	100	0	-
MON	100	0	-
Cetane Number	-	-	44.5
MW	114.23	100.20	-

2.2 Data Acquisition and Analysis Methodology

All of the measured data were recorded in a custom, in-house LabView data acquisition system with real-time combustion performance monitoring. Once the combustion reached steady-state, 300 consecutive cycles were recorded. A custom-made Matlab script is employed for high accuracy post-processing of the experimental data. For example, Equation (2) can be used to calculate the net heat release rate (NHRR) of each cycle from the cylinder pressure measurements.

$$NHRR\left[\frac{J}{CA}\right] = \frac{\gamma * pdV}{\gamma - 1} + \frac{VdP}{\gamma - 1} \quad (2)$$

Heat transfer losses to the walls, cylinder head, and piston are calculated by using the Chang heat transfer correlation [33] in the convective heat transfer equation:

$$HT = h * Area * (T_{bulk} - T_{wall}) \quad (3)$$

where h is the convective heat transfer coefficient. The Chang heat transfer correlation relates h to the engine speed, cylinder temperature and pressure, displaced volume, etc. By adding heat transfer losses to the NHRR, the gross heat release rate (GHRR), which is the energy release rate due to combustion, is found. During the post processing, the heat transfer coefficient is scaled by the energy enclosure method, which is calculated from the fuel lower heat value and amount of fuel injected into the cylinder through the cycle. By integrating the GHRR with respect to crank angle and then normalizing by the total cumulative heat release, the mass fraction burned (MFB) curve is produced, which indicates the fraction of fuel that has been burned at a given crank angle. In this work, the start of combustion is defined as CA10, which is the crank angle at which ten percent of fuel has burned; combustion phasing was defined as CA50, which is the crank angle when half of the fuel has burned. The burn duration was defined as the crank angle duration between CA10 and CA90.

2.3 Engine operating conditions

The engine was operated at 1200 rpm for all of the experimental results presented in this paper, and a nominal total fuel flow rate of 10 mg/cycle was maintained by controlling the DI and PFI injection durations as constant. The engine load is mainly dictated by the fuel flow rate, and therefore, the load was kept at a relatively constant value throughout all of the experiments. Applying external-cooled EGR does not have a significant effect on the engine load; however, it significantly changes the equivalence ratio without changing the overall level of fuel dilution in the cylinder. Thus, a charge-mass equivalence ratio, ϕ', is introduced. This charge-mass equivalence ratio is defined by the following equation:

$$\phi' = \phi * \left(1 - \frac{EGR+RGF}{100}\right) \quad (4)$$

where ϕ is the detected and calculated equivalence ratio (from a lambda sensor and the emissions bench based on exhaust composition), and RGF represents the internal residual gas fraction, which is the portion of the trapped mass that is residual gases from the previous cycle, and EGR is the percent of external-cooled EGR that was used. In other words, ϕ also can be considered as the in-cylinder fuel equivalence ratio when there is no EGR applied since the RGF is relatively small in a high compression ratio engine. ϕ' can be considered as the in-cylinder fuel dilution considering air and residual gases as diluents. The charge-mass equivalence ratio, ϕ', was maintained at 0.32 ± 0.02 across all of the experiments. Other engine operating conditions can be found in *Table3*.

Table 3: ENGINE OPERATING CONDITIONS

Engine Speed [rpm]	1200
Nominal Load Range (IMEPg) [bar]	3.6 to 3.9
PFI Fuel	PRF50 to PRF90
PFI Fuel Injection Timing [deg aTDC]	-120
PFI Injection Duration [ms]	3.5
PFI Pressure [psi]	28
DI Fuel	Diesel
DI Fuel Injection Timing Window [deg aTDC]	-65 to -45
DI fuel Injection Duration [CAD]	0.14
DI Rail Pressure [bar]	730
Blend Ratio by Energy [%]	76 ± 2
Total Fuel Rate [g/s]	0. 1 ± 0.03
Intake Pressure [bar]	1.01 ± 0.01
Intake Temperature [K]	320 ± 0.5
Exhaust Pressure [bar]	1.16 ± 0.3
EGR [%]	Sweep
Charge-Mass Equivalence Ratio (ϕ')	0.32 ± 0.02

For safety reasons, a cylinder peak pressure limit of 110 bar was abided by, and the peak pressure rise rate (PPRR) was limited to less than 10 bar per crank angle degree (CAD). In addition, based on cycle-to-cycle stability, the coefficient of variation of $IMEP_n$ (COV of $IMEP_n$) was limited to less than 5%. The operating load range varied from misfire, when combustion efficiency was excessively low and the COV began to exceed 5%, to knocking mostly with high reactivity port injected fuels, when the PPRR began to exceed 10 bar/ CAD.

3. RESULTS AND DISCUSSION

3.1 Effects of varying the reactivity of the premixed fuel in RCCI

In order to investigate the effect of the reactivity separation between the low and high reactivity fuels (i.e., the premixed and directed injected fuels, respectively), the port injected fuel's reactivity was varied by using different PRF number blends as the premixed fuel. In all of the experiments in this paper, the direct injected fuel is an EPA certification ultra-low sulfur diesel (ULSD). The injection timing window, injection strategy, intake and exhaust pressure, intake temperature and the amount of fuel were held constant, which is shown in Table 3. The EGR fraction was used to ensure that the maximum pressure rise rate remained below the knocking limit (10 bar/crank angle degree), especially when a high reactivity fuel (lower PRF number) was port injected. However, the EGR fraction was limited to avoid excessively low combustion efficiencies. In general, for the same injection timing window, the EGR fraction decreases with increasing PRF number of the port injected fuel. In this section, only a few conditions are chosen to be analyzed, and additional operating condition sweeps and performance characteristics can be found in the Appendix.

The effect of port injected fuel reactivity on ignition timing (CA10) and combustion phasing (CA50)

With the same injection timing window and EGR fraction, the variation in premixed fuel reactivity (i.e., PRF number) has a significant effect on the combustion phasing (CA50). As the premixed fuel reactivity decreases, CA50 is considerably retarded. This is because of two reasons. First, an increase in PRF number leads to the increase in auto-ignition resistance. Higher auto-ignition resistance requires higher temperatures to initiate combustion either through heat release from the diesel fuel or through more compression work; both of which take time. Second, there is low temperature heat release (LTHR), which will be shown later, that comes from both the direct injected diesel fuel, and the premixed fuel. Both DI and PFI fuels are held at constant flow rates, but the lower PRF number premixed fuels contribute more to the LTHR due to a larger portion of n-heptane. This causes the combustion phasing of the high temperature heat release (HTHR) to advance. Therefore, the ignition timing advances as the PRF number of the premixed fuel decreases. Consequently, CA50 advances as well.

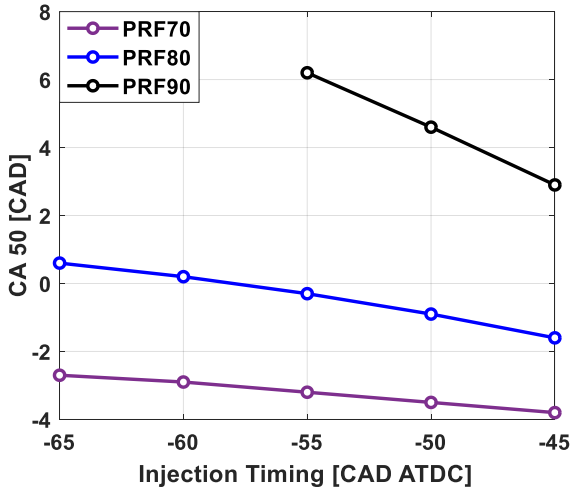

Figure 4: CA50 FOR DIFFERENT PRF BLENDS AS THE PREMIXED FUEL VS. INJECTION TIMING

Interestingly, the effect of injection timing on combustion phasing gets stronger as the PRF number of the premixed fuel increases, which means the combustion phasing is advanced more with the same retardation of SOI timing under higher reactivity fuel blends. As shown in *Figure 4*, the slope of each trendline, which can be considered as the sensitivity of combustion phasing to injection timing, increases as the PRF number increases. This trend can also be observed in *Figure 5* and *6*. Each connected line has the same injection timing, and each PRF fuel has three lines, which indicates the three injection timings: -45, -55 and -65 degrees aTDC. As the PRF number increases, the gap between the lines increases, which means the effect of injection timing gets stronger.

This enhancement of injection timing sensitivity is caused by the increasing separation between the premixed and DI fuels, which increases the reactivity stratification (or reactivity gradients) in the cylinder. In RCCI, the ignition timing and burn duration are dictated by the injection timing and corresponding stratification of diesel fuel, and by the reactivity separation between the DI and premixed fuels. These results show that the sensitivity of the RCCI combustion phasing to injection timing is higher when there is a larger reactivity separation between the premixed and DI fuels. The specific reasons for the heightened sensitivity to injection timing when the reactivity separation increses are discussed in more detail in the following paragraphs.

At a lower PRF numbers, both the PFI and DI fuel have a low auto-ignition threshold. Thus, they are both able to auto-ignite at relatively low temperatures. Regardless of the injection timing, the temperatures before TDC are already high enough for auto-ignition to occur in the rich regions in the cylinder. When the reactivity separation is lower, the reactivity of the lower reactivity regions is not significantly different than the high reactivity regions. Therefore, these lower reactivity region only need a small amount of heat release to reach auto-ignition. Thus, retarding the injection timing does not have a strong effect with the higher reactivity premixed fuels. Additionally, the LTHR increases for the low PRF numbers blends, which is a contributing factor to the lower sensitivity of the low PRF number fuels to injection timing.

As the PRF number increases, the reactivity seperation between the premixed and DI fuels increases, the global reactivity decreases, and the injection timing starts to play a more important role. Because the background premixed fuel has a higher resistance to auto-ignition, the injection timing and level of mixedness of the high reactivity fuel has a much larger effect on the combustion characteristics.

Beyond the differences in sensitivity of the combustion process to the injection timing at different premixed fuel reactivities, *Figure 5* and *6* display strong trends between the combustion efficiency or gross thermal efficiency with the EGR fraction, injection timing, and PRF number. These differences will be explored in detail in the remainder of the paper.

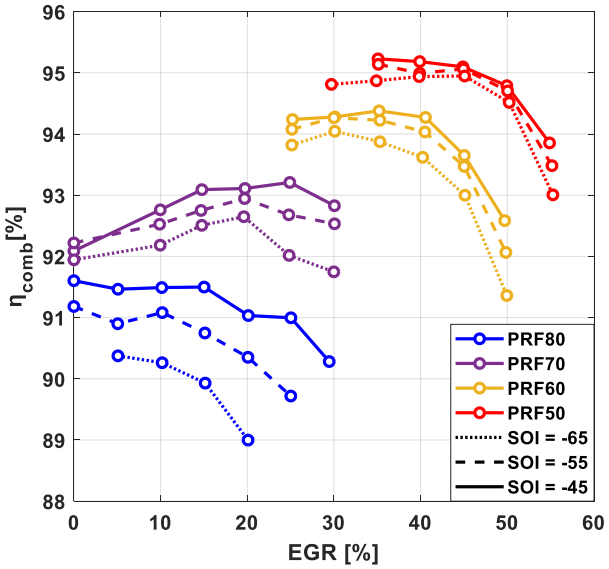

Figure 5: COMBUSTION EFFICIENCY VS. EGR WITH DIFFERENT PRF BLENDS AS THE PREMIXED FUEL

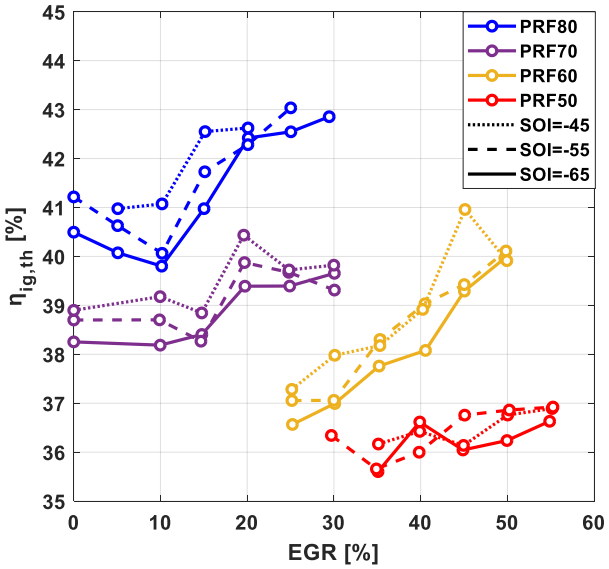

Figure 6: GROSS INDICATED THERMAL EFFICIENCY VS. EGR WITH DIFFERENT PRF BLENDS AS THE PREMIXED FUEL AND DIFFERENT INJECTION TIMINGS

The effect of premixed fuel reactivity on combustion efficiency, gross indicated thermal efficiency, and emissions

Figure 7 shows the combustion efficiency, gross indicated thermal efficiency, and fuel conversion efficiency versus combustion phasing (CA50). The combustion efficiency is defined as the percent of the injected fuel that burned. The gross indicated thermal efficiency considers the work produced by the engine as a fraction of the fuel that burned, because the fuel that burned constitutes the energy that was added to the thermodynamic cycle. Alternatively, the fuel conversion efficiency considers the work produced by the engine as a fraction of the total fuel energy that was injected. The fuel conversion efficiency is the product of indicated thermal

efficiency and the combustion efficiency. These definitions can be found in Heywood [1].

Each point of the same color represents a different premixed fuel reactivity. The aim of this section is to examine the effect of CA50 and fuel reactivity on efficiencies. Two trends of combustion efficiency are seen in *Figure 7 (a)*: first, the combustion efficiency remains nearly constant before a CA50 of 0 crank angle degrees, but starts decreasing when CA50 was retarded. This is due to the instantaneous piston motion while combustion is occuring, which affects all low temperature combustion modes. The volume expansion counteracts the compression effect from combustion elsewhere in the cylinder (as opposed to aiding it when combustion occurs before TDC). Due to the conventional diesel-style re-entrant bowl piston geometry, the diesel injector's included angle, and the relatively early direct injection timing of RCCI, the direct injected fuel targets the periphery of the cylinder, outside of the piston bowl. Thus, the combustion efficiency could be improved with a specifically designed injector included angle and/or piston bowl geometry. Second, the combustion efficiency decreases as the PRF number of PFI fuel is increased by 8.6% from the highest value of 95.23% to the lowest value of 87.05%. This can be explained by the varying reactivity of the premixed fuel. As the PRF number increases, the global reactivity decreases, and the resistance to auto-ignition increases. As a result, a larger percentage of the fuel in cold regions will not start or complete the combustion process with higher PRF numbers.

The gross indicated thermal efficiency was calculated from the following equation from Heywood [1]:

$$\eta_{ig,\mathrm{th}} = \frac{W_{\mathrm{ig}}}{m_{fuel} * Q_{lhv} * \eta_{\mathrm{comb}}} \quad (5)$$

where W_{ig} is the gross indicated work per cycle, calculated from the cylinder pressure data, and m_{fuel} is total fuel injected per cycle. The gross indicated thermal efficiency is independent of combustion efficiency. The gross thermal efficiency is representative of the efficiency of the closed portion of the thermodynamic cycle.

The gross indicated thermal efficiency is closely coupled with CA50 during this study. In *Figure 7 (b)*, it can be seen that the gross indicated thermal efficiency increases as CA50 retards. Across all combustion modes, there is a tradeoff between heat transfer losses and expansion work that causes an efficiency optimum with combustion phasing. This effect is well documented in the literature and this optimum typically occurs when CA50 is around 8-10 degrees aTDC for a light-duty engine [1]. However, in this study, the CA50 is not able to occur later than 7 degrees aTDC due to a significant decrease in combustion efficiency and an increase in COV of IMEPn. These results indicate that it is not possible to delay the CA50 combustion phasing of RCCI beyond approximately 7 degrees in a light-duty engine without excessive unburned hydrocarbon and CO emissions and cyclic variability.

Some other experimental RCCI results have shown the expected trend of gross thermal efficiency [34] (i.e., an optimum with combustion phasing). The main reason for this difference is the engine displacement used for this study. It has been shown that with larger engine displacements, the fraction of total heat release that is lost to heat tranfer is lower [1], thus shifting the optimum earlier in combustion phasing than observed here.

Figure 7 (b) also shows that there is a strong trend between PRF number of the premixed fuel and the gross indicated thermal efficiency. The gross indicated thermal efficiency increased by up to 22%, from the lowest value of 35.28% to the highest value of 43.04%, and the peak efficiency happens at PRF80. The exact reason for this trend of efficiency with PRF number will be explored in detail later in this paper.

The fuel conversion efficiency is the product of indicated thermal efficiency and combustion efficiency, which is shown in Equation (6):

$$\eta_{\mathrm{ig,f}} = \eta_{ig,\mathrm{th}} * \eta_{\mathrm{comb}} = \frac{W_{\mathrm{ig}}}{m_{fuel} * Q_{lhv}} \quad (6)$$

In *Figure7 (c)*, the gross fuel conversion efficiency initially increases because of the increase in gross indicated thermal efficiency and nearly constant combustion efficiency, and then decreases once the decrease in combustion efficiency outweighs the increase in gross indicated thermal efficiency. In the case of PRF90, 80, 60, and 50, the gross fuel conversion efficiency exhibits a broad optimum with the peak around a CA50 of 3 degrees aTDC. However, the case of PRF70 has an earlier peak at 0 degrees aTDC. This could be due to experimental variability. For example, compared with the other PRF number cases, PRF70 had a slightly lower load and charge-mass equivalence ratio, which can be seen in the *Appendix*. Overall, PRF80 has the highest fuel conversion efficiency, which peaked at 38.8%. *Figure 7 (b)* also shows that when CA50 is constant, an increase in PRF number of the premixed fuel leads to an increase in gross indicated thermal efficiency from PRF50 to 80.

In order to investigate this thoroughly, a subsample of the data set is further analyzed in the next section. The key features of this subsample are shown in *Table 4* and the pressure and heat release for the four operating conditions are shown in Figure 8. In this subsample, all of the operating conditions have a similar CA50 combustion phasing of -0.8 degrees aTDC, which was achieved by varying the EGR level and SOI timing at the different PRF number cases. The combustion efficiency decreases from 95.06% to 91.41% as the PRF number increases, as illustrated above. The other main differences are the EGR percentage, which decreased from 45% to 0%. In order to achieve the same CA50, the higher reactivity fuels (lower PRF number) require a larger portion of EGR, which effectively retards combustion phasing. However, EGR also changes the mixture's properties, such as the ratio of specific heats, γ, and lowers the cylinder temperature, which reduces heat transfer losses. The trends in gross indicated thermal efficiency shown in Figure 7 (increasing from PRF50 to 80 and then decreasing from

80 to 90) is the combined, competing effects of heat transfer losses and changes to the mixture properties. Interestingly, the heat release characteristics for the four different cases compared in Figure 8 are surprisingly similar. It is hypothesized that the lower EGR fraction and larger reactivity separation are counter-balancing each other, resulting in a similar heat release process across the four cases.

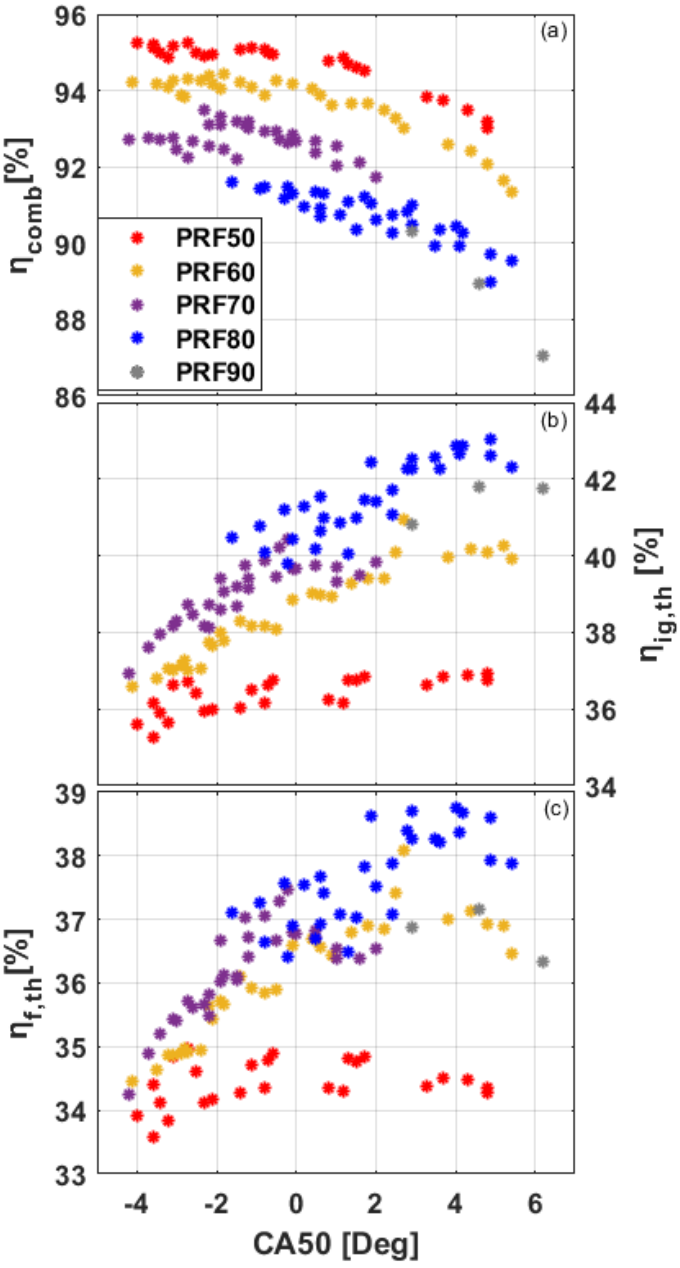

Figure 7: (A) COMBUSTION EFFICIENCY, (B) GROSS INDICATED THERMAL EFFICIENCY, AND (C) FUEL CONVERSION EFFICIENCY VS. CA50

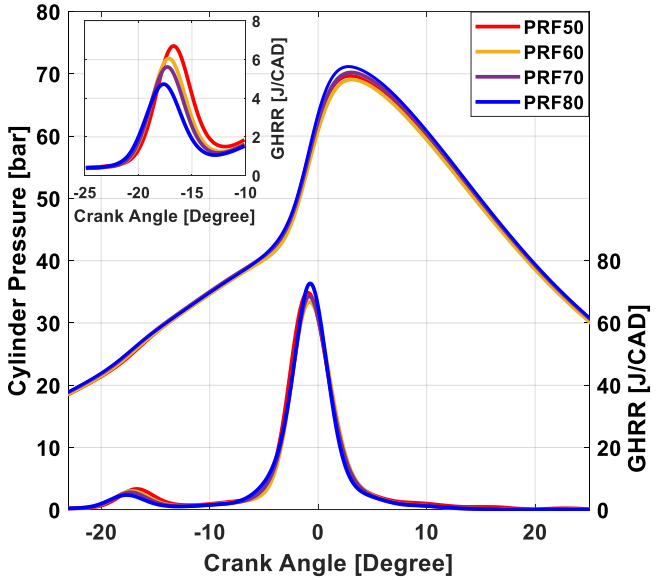

Figure 8: GROSS HEAT RELEASE RATE (GHRR, BOTTOM) & CYLINDER PRESSURE (TOP) VS. CAD

Table 4: COMBUSTION CHARACTERISTICS FOR THE PRF BLEND SUBSAMPLE STUDY

PRF Number	50	60	70	80
Injection Timing [CAD ATDC]	-55	-65	-55	-50
IMEPg [bar]	3.72	3.64	3.68	3.70
Combustion Efficiency [%]	95.06	93.87	92.94	91.41
Gross Indicated Thermal Conversion Efficiency [%]	36.14	38.18	39.87	40.77
Gross Indicated Fuel Conversion Efficiency [%]	34.35	35.84	37.06	37.27
EGR [%]	45	35	20	0
CA 50 [CAD ATDC]	-0.8	-0.8	-0.8	-0.9
Total Fuel flow [g/s]	0.103	0.095	0.095	0.095
Phi Prime	0.34	0.31	0.31	0.31
Blend Ratio [by Energy]	0.78	0.78	0.77	0.76

The emissions for the four comparison cases listed in *Table 4* are shown in *Figure 9*. When the premixed fuel's reactivity decreases, the UHC and CO emissions increased by 77% and 58%, respectively. There are two reasons for this trend. First, the auto-ignition resistance increases as the PRF number increases and the quenching area such as the regions close to the walls as well as the crevice volumes will not be oxidized completely. Second, with the increase in PRF number, the required EGR percentage decreased from 45% to 0, which has

several effects on combustion and emissions. With similar combustion phasing, higher EGR percentages led to higher combustion efficiencies across all combustion modes because a fraction of the unburned fuel is recirculated and gets another chance to burn. The CO emissions highly depends on the peak bulk temperature to produce sufficient OH radicals. The NOx emissions increased because the cylinder temperature increases due to lower heat capacity of fresh air compared with EGR.

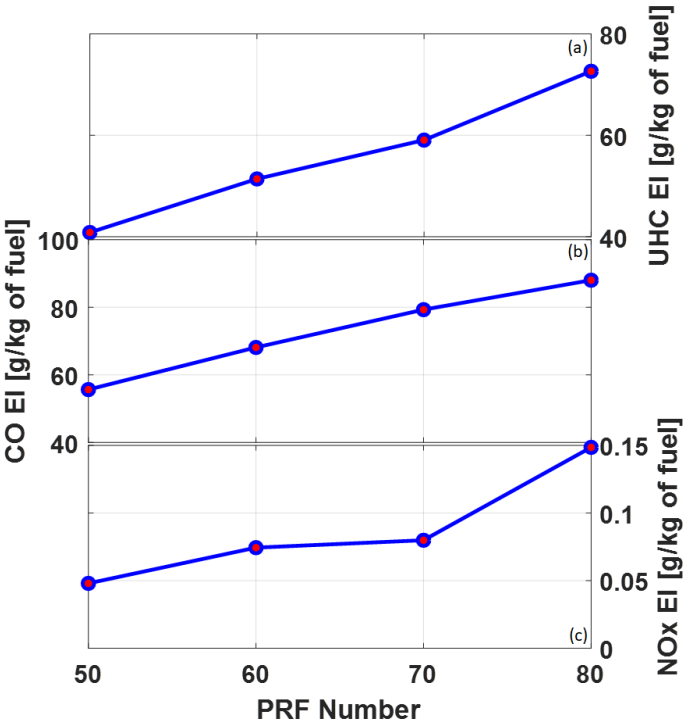

Figure 9: (A) UNBURNED HYDROCARBON EMISSIONS, (B) CO EMISSIONS, AND (C) NOX EMISSIONS VS. PRF NUMBER

3.2 RCCI injection timing and EGR study

The effect of injection timing on ignition timing (CA10), combustion phasing (CA50), and heat release rate

During this experimental injection timing and EGR study, the load (IMEPg) is fixed by maintaining a constant fuel flow rate. Additionally, the intake temperature, intake pressure, and exhaust pressure are kept constant, which is shown in Table 3. The injection timing window was -65 degrees to -45 degrees aTDC in increments of 5 degrees. This injection timing window was selected because it is the range that is relevant for RCCI combustion [35]. Further retarding injection timing begins to transition to conventional dual-fuel combustion with diesel-like diffusion flames [36]. If the injection timings are significantly earlier, the diesel injection becomes too premixed and loses its ability to control combustion phasing in RCCI. As a result, the combustion process approaches dual-fuel HCCI combustion. Although the total injection range is approximately -65 to -45 degrees aTDC, some fuel/EGR combinations have a narrower injection timing window in order to obey the combustion limits described above (peak pressure rise rate limit and COV of IMEPn). An example injection timing comparison for PRF80 and 15% EGR is shown in Figure 10.

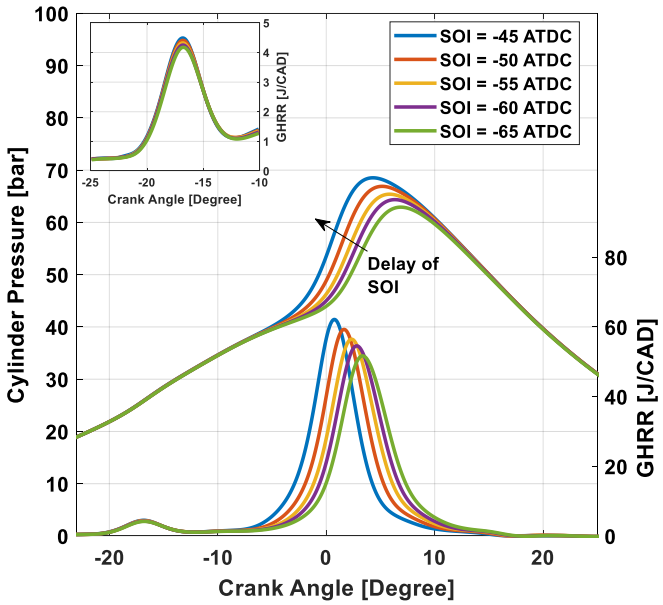

Figure 10: GROSS HEAT RELEASE RATE (GHRR, BOTTOM) & CYLINDER PRESSURE (TOP) VS. CAD FOR PRF80 WITH 15% EGR

It can be observed that the later injection timings have earlier combustion phasings (due to the richer diesel regions around TDC which will be explained later), while the earlier injection timings have later CA50 (due to more mixing). As shown in *Figure 11*, the load (IMEPg) was the same at each injection timing. As the injection timing was retarded from -65 to -45 degrees aTDC, the ignition timing (CA10) and combustion phasing (CA50) advanced from 3.5 to 0.7 degrees aTDC for CA50. This is a common characteristic of RCCI combustion due to the differences in the local equivalence ratio distribution and reactivity separation caused by the different diesel injection timings (i.e., the richer diesel regions auto-ignite earlier). The later injection timings result in earlier combustion phasing because when the injection timing is retarded, there is less time for the direct injected fuel to mix with background fuel before ignition. This results in an earlier start of combustion timings for the latest injection timings. Once ignition starts, the heat release and compression from combustion elsewhere in the cylinder further increases the cylinder temperature, causing the lower reactivity regions to auto-ignite. As the start of combustion and CA50 advance, the burn duration decreases and the peak heat release rate increases. This agrees well with the observed peak pressure rise rate (PPRR) in *Figure 11*. When the injection timing was -65 degrees aTDC, the PPRR was 4.4 bar/deg. As the injection timing retarded to -45 degrees aTDC, the PPRR increased to 5.9 bar/deg.

Contrarily, the early injection event leads to later ignition timings and combustion phasings. This is because when injection timing is advanced, the direct injected fuel has more

time to mix with the air and the low reactivity background fuel. Increased mixing reduces the local richness and lowers the reactivity gradient, which prolongs the ignition delay.

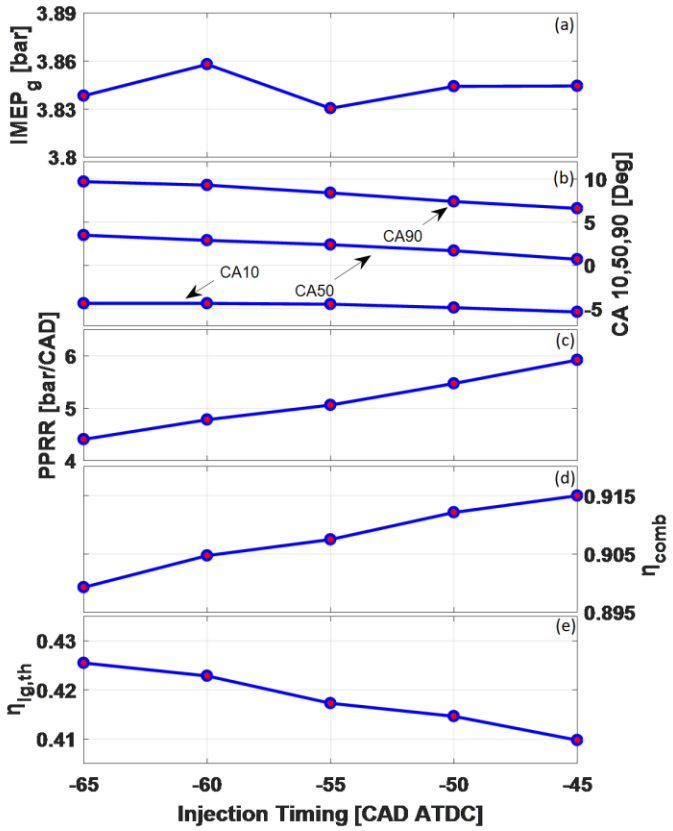

Figure 11: (A) IMEPG, (B)CA10, 50, & 90, (C) PEAK PRESSURE RISE RATE, (D) COMBUSTION EFFICIENCY, AND (E) GROSS INDICATED THERMAL EFFICIENCY VS. INJECTION TIMING

The effect of injection timing on combustion efficiency, gross indicated thermal efficiency, and emissions

For the comparison in Figure 10, the results for the gross load, combustion phasings, PPRR, combustion efficiency, and indicated gross thermal efficiency are shown in Figure 11. The emissions, including the Emissions Index (EI) unburned hydrocarbon (UHC) emissions, EI CO emissions, and EI NOx emissions, are shown in Figure 12. The combustion efficiency increased from 89.9% to 91.5% when the injection timing was delayed from -65 to -45 degrees aTDC. This is attributed to the higher heat release rates and earlier combustion phasings associated with later injection timings, which leads to higher in-cylinder temperatures and agrees with the observed decrease in UHC and CO emissions by 10.7% and 23.2%, respectively. Contrarily, the gross indicated thermal efficiency appears to have a significantly different trend compared to the combustion efficiency. Due to the advance in combustion phasings toward TDC, the gross indicated thermal efficiency decreased from 42.55% to 40.98%. Meanwhile, the NOx emissions were doubled as the injection timing delayed from -65 deg ATDC to -45 deg aTDC because of the higher temperatures and higher equivalence ratio regions at the time of combustion.

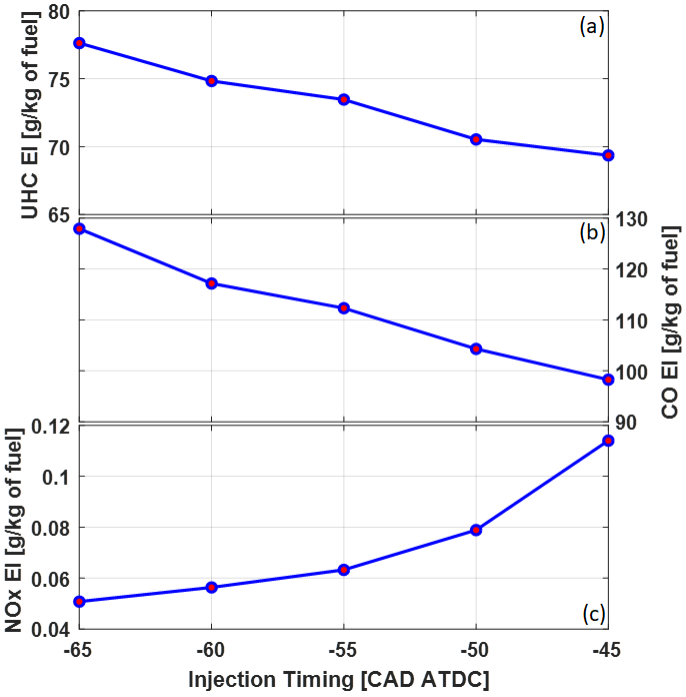

Figure 12: (A) UNBURNED HYDROCARBON EMISSIONS, (B) CO EMISSIONS, AND (C) NOX EMISSIONS VS. INJECTION TIMING

The effect of EGR on ignition timing (CA10), combustion phasing (CA50), and heat release rate

In this section, the EGR fraction was varied while other operating conditions, such as the injection timing of the DI fuel, the intake temperature, the intake pressure, the exhaust pressure, the blend ratio, and the total fuel flow rate, were held constant, which is shown in Table 3.

The EGR percentage increased from 25% to 50% in increments of 5% and the results are shown in ***Figure 13***. It can be observed that the effect of EGR on combustion is much stronger than injection timing, when compared with ***Figure 10***. As the EGR increased, the start of the high-temperature heat release (HTHR) retarded, and the duration of the HTHR increased. Meanwhile, there is a significant reduction in the peak heat release rate. The LTHR has the same trend as the high-temperature heat release. It has been shown that the ignition timing and the total amount of LTHR is effectively regulated by EGR [38]. Due to its composition of H_2O and CO_2, EGR has a higher ratio of specific heats, which raises the amount of thermal energy to reach the same temperature; as a result, the temperature of the mixture decreases, which explains the delayed heat release.

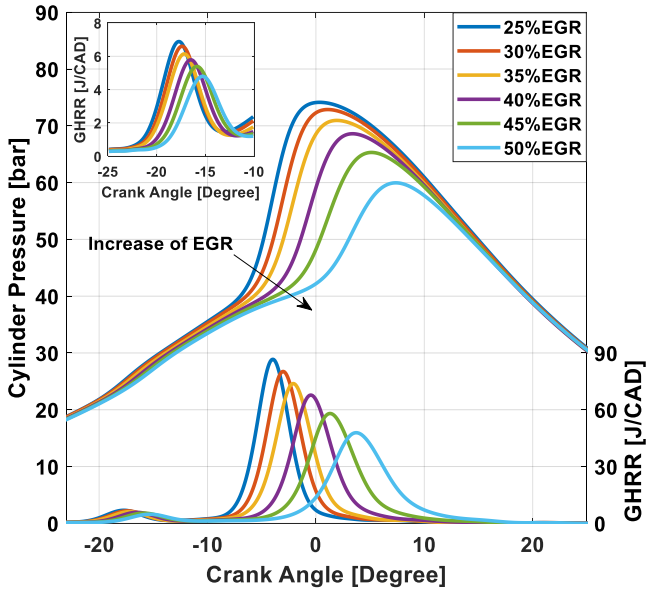

Figure 13: GROSS HEAT RELEASE RATE (GHRR, BOTTOM) & CYLINDER PRESSURE (TOP) VS. CAD FOR PRF60 AT AN SOI OF 45 DEGREES BTDC

The effects of applying EGR in RCCI is similar to that in HCCI [38]. In *Figure 14*, it can be seen that there is a slight increase in load with EGR, and the load ranged from 3.6 to 3.78 bar is caused by experimental variation. The ignition timing (CA10) and combustion phasing were delayed considerably. There are two main reasons for this. First, as discussed above, EGR can be regarded as a high heat capacity reservoir. Since the ignition timing is strongly dependent on temperature, when the EGR fraction increases, the in-cylinder temperature decreases. Thus, the ignition timing is delayed. Second, using EGR leads to a lower oxygen concentration in the mixture, because fresh air is displaced by external-cooled EGR. The concentration of oxygen plays an important role in the ignition delay and reactivity of the mixture where lower concentrations of oxygen result in later ignition. Due to the delay of CA10 (from -11.3 to -4.7 degrees aTDC), the CA50 was also delayed (from -4.1 to 3.8 degrees aTDC). Moreover, it can be seen that the duration between CA10 and CA90 increases as the EGR increases. The increase in burn duration was also shown in the GHRR in *Figure 13*.

The effect of EGR on combustion efficiency, gross indicated thermal efficiency, and emissions

From the combustion efficiency results in *Figure 14*, it can be seen that there is a slight increase from 94.2% to 94.4% as the EGR is increased from 25% to 35%, followed by a decrease to 92.6% as the EGR increased further to 50%. As shown in [39], EGR has several effects on combustion. Applying EGR gives the unburned fuel from the previous cycle another chance to burn, which explains the slight increase from 25% to 35% EGR. However, increasing the amount of EGR also decreases the overall cylinder temperature and the oxygen concentration, and delays combustion phasing. This can result in regions whose local temperatures never reach the auto-ignition threshold, resulting in a dramatic decrease in the combustion efficiency.

In *Figure 5 & 6*, it can be seen that a larger amount of EGR must be utilized with the lower PRF number premixed fuels to achieve the desired combustion phasing. Within each PRF blend, the combustion efficiency-EGR trend outlined in Figure 14 occurs in Figure 5 (i.e., a slight increase in combustion efficiency as the EGR increased followed by significant decrease as the EGR level increases further due to delayed combustion phasing and over-elongated burn durations). As the PRF number increases to 80, the fuel's higher resistance to auto-ignition shifts the combustion phasing later and dominates the tradeoff of combustion efficiency.

As shown in *Figure 14*, the gross indicated thermal efficiency increases as the EGR percentage increases. This phenomenon is mainly caused by two effects. First, the combustion phasing is retarded to a more efficient timing. The experimental results showed that gross indicated thermal efficiency is closely coupled with CA50, which was discussed in the reactivity separtion section above. Second, increases in EGR considerably lower the peak bulk temperature, which increases the ratio of the specific heats (gamma) and reduces heat transfer losses, both of which result in higher gross indicated thermal efficiencies. The emissions data, shown in *Figure 15*, agreed with the analysis above.

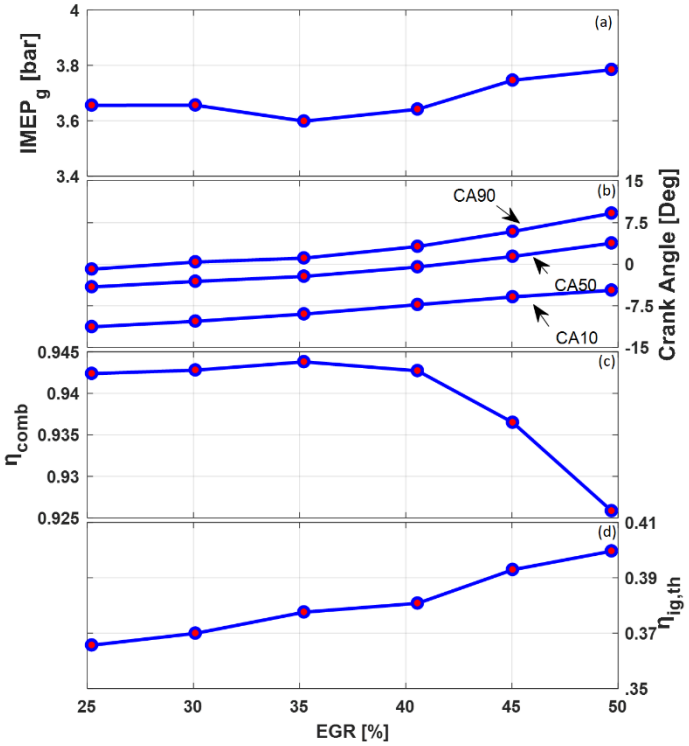

Figure 14: (A) IMEPG, (B) CA10, 50, & 90, (C) COMBUSTION EFFICIENCY, (E) GROSS INDICATED THERMAL EFFICIENCY VS. EGR FRACTION FOR PRF60 AT AN SOI OF 45 DEGREES BTDC

Figure 15 shows the trends of emissions with EGR percentage. The NOx emissions decreased by 54% due to lower peak temperatures which was caused by three factors; the lower peak heat release, the longer heat release duration, and the higher heat capacity of the EGR (compared to excess air). Therefore, the NOx emissions significantly decrease with increasing EGR rate.

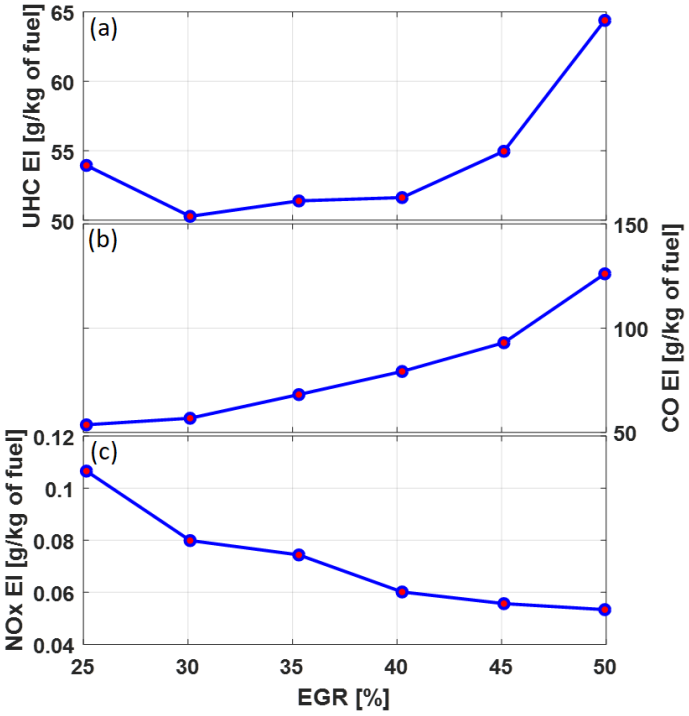

Figure 15: (A) UNBURNED HYDROCARBON, (B) CO EMISSIONS, AND (C) NOX EMISSIONS VS. EGR FRACTION FOR PRF60 AT AN SOI OF 45 DEGREES BTDC

4. CONCLUSIONS

An experimental study of RCCI combustion was conducted on a single cylinder light-duty diesel engine. The experiments were designed to better understand the reactivity separation between the high and low reactivity fuels, the effects of injection timing, and the effects of EGR fraction on the combustion and emissions characteristics of RCCI combustion. The results can be divided into three parts; a reactivity separation study, an injection timing study, and an EGR study. The conclusions are as follows.

With the same EGR and injection timing conditions, a decrease in the port injected fuel's reactivity (or increase in the PRF value) results in:

1. Considerably delayed ignition timing and combustion phasing.
2. Decrease in combustion efficiency and increase in gross indicated thermal efficiency. The fuel conversion efficiency increases first, then decreases.
3. An increased sensitivity to DI injection timing.
4. The combustion efficiency and gross indicated thermal efficiency are closely coupled with CA50. Delaying CA50 decreases the combustion efficiency and increases the gross indicated thermal efficiency. This is an important consideration and an inherent tradeoff of RCCI combustion, which causes the fuel conversion efficiency to increase first, and then decrease.

In order to investigate the effects of the port injected fuel reactivity on combustion, and decouple the CA50 effects, a subsample of data was chosen with same CA50. Decreasing the port injected fuel's reactivity (or increasing the PRF value of the PFI fuel) has the following effects:

1. Decrease in the total amount and rate of LTHR.
2. Decrease in the combustion efficiency and increase in the gross indicated thermal efficiency.
3. Decrease in the ability to apply more EGR and shorten the burn duration.
4. Increase in the UHC, CO, and NOx emissions.

Delaying injection timing results in:

1. Earlier ignition timing and combustion phasing.
2. Higher combustion efficiency and decreased gross indicated thermal efficiency.
3. Higher peak cylinder pressure, peak pressure rise rate, peak in-cylinder temperature, and peak heat release rate.
4. Lower UHC and CO emissions and higher NOx emissions.

Increasing the percentage of EGR:

1. Delays the ignition timing and combustion phasing.
2. Lowers the peak in-cylinder temperature, pressure, and heat release rate, and prolongs the burn duration.
3. Increases the combustion efficiency initially, and then decreases the combustion efficiency for high reactivity premixed fuels. For the low reactivity fuel, increasing the EGR percentage only decreases the combustion efficiency.
4. Increases the gross indicated thermal efficiency.
5. Increases the CO, UHC, and decreases the NOx emissions.

5. ACKNOWLEDGEMENTS

This work was partially supported by the Department of Energy under award number DE-EE0007216.

REFERENCES

[1] Heywood, J.B., 2018. Internal combustion engine fundamentals, New York: McGraw-Hill Education.

[2] Gu, X., Huang, Z., Cai, J., Gong, J., Wu, X. and Lee, C.F., 2012. Emission characteristics of a spark-ignition engine fuelled with gasoline-n-butanol blends in combination with EGR. Fuel, 93, pp.611-617.

[3] Hsieh, W.D., Chen, R.H., Wu, T.L. and Lin, T.H., 2002. Engine performance and pollutant emission of an SI engine using ethanol–gasoline blended fuels. Atmospheric Environment, 36(3), pp.403-410.

[4] Lapuerta, M., Armas, O. and Rodriguez-Fernandez, J., 2008. Effect of biodiesel fuels on diesel engine emissions. Progress in energy and combustion science, 34(2), pp.198-223.

[5] Choi, C.Y. and Reitz, R.D., 1999. An experimental study on the effects of oxygenated fuel blends and multiple injection strategies on DI diesel engine emissions. Fuel, 78(11), pp.1303-1317.

[6] Ran, Z., Hariharan, D., Lawler, B. and Mamalis, S., 2019. Experimental study of lean spark ignition combustion using gasoline, ethanol, natural gas, and syngas. Fuel, 235, pp.530-537.

[7] Dec, J.E., 2009. Advanced compression-ignition engines—understanding the in-cylinder processes. Proceedings of the combustion institute, 32(2), pp.2727-2742.

[8] Sjöberg, M., Dec, J.E., Babajimopoulos, A. and Assanis, D., 2004. Comparing enhanced natural thermal stratification against retarded combustion phasing for smoothing of HCCI heat-release rates. SAE transactions, pp.1557-1575.

[9] Dec, J.E. and Sjöberg, M., 2003. A parametric study of HCCI combustion—the sources of emissions at low loads and the effects of GDI fuel injection. SAE transactions, pp.1119-1141.

[10] Persson, H., Hultqvist, A., Johansson, B. and Remón, A., 2007. Investigation of the early flame development in spark assisted HCCI combustion using high speed chemiluminescence imaging (No. 2007-01-0212). SAE Technical Paper.

[11] Hessel, R.P., Foster, D.E., Aceves, S.M., Davisson, M.L., Espinosa-Loza, F., Flowers, D.L., Pitz, W.J., Dec, J.E., Sjöberg, M. and Babajimopoulos, A., 2008. Modeling iso-octane HCCI using CFD with multi-zone detailed chemistry; comparison to detailed speciation data over a range of lean equivalence ratios (No. 2008-01-0047). SAE Technical Paper.

[12] Yang, R., Hariharan, D., Zilg, S., Lawler, B. and Mamalis, S., 2018. Efficiency and emissions characteristics of an HCCI engine fueled by primary reference fuels. SAE International Journal of Engines, 11(2018-01-1255), pp.993-1006.

[13] Hariharan, D., Yang, R., Zhou, Y., Gainey, B., Mamalis, S., Smith, R.E., Lugo-Pimentel, M.A., Castaldi, M.J., Gill, R., Davis, A. and Modroukas, D., 2019. Catalytic partial oxidation reformation of diesel, gasoline, and natural gas for use in low temperature combustion engines. Fuel, 246, pp.295-307.

[14] Inagaki, K., Fuyuto, T., Nishikawa, K., Nakakita, K. and Sakata, I., 2006. Dual-fuel PCI combustion controlled by in-cylinder stratification of ignitability (No. 2006-01-0028). SAE Technical Paper.

[15] Simescu, S., Fiveland, S.B. and Dodge, L.G., 2003. An experimental investigation of PCCI-DI combustion and emissions in a heavy-duty diesel engine (No. 2003-01-0345). SAE Technical Paper.

[16] Kokjohn, S., Reitz, R., Splitter, D. and Musculus, M., 2012. Investigation of fuel reactivity stratification for controlling PCI heat-release rates using high-speed chemiluminescence imaging and fuel tracer fluorescence. SAE International Journal of Engines, 5(2), pp.248-269.

[17] Gainey, B., Hariharan, D., Yan, Z., Zilg, S., Rahimi Boldaji, M. and Lawler, B., 2018. A split injection of wet ethanol to enable thermally stratified compression ignition. International Journal of Engine Research, p.1468087418810587.

[18] Boldaji, M.R., Sofianopoulos, A., Mamalis, S. and Lawler, B., 2018. Effects of Mass, Pressure, and Timing of Injection on the Efficiency and Emissions Characteristics of TSCI Combustion with Direct Water Injection (No. 2018-01-0178). SAE Technical Paper.

[19] Splitter, D., Hanson, R., Kokjohn, S., Wissink, M. and Reitz, R.D., 2011. Injection effects in low load RCCI dual-fuel combustion (No. 2011-24-0047). SAE Technical Paper.

[20] DelVescovo, D., Kokjohn, S. and Reitz, R., 2017. The effects of charge preparation, fuel stratification, and premixed fuel chemistry on reactivity controlled compression ignition (RCCI) combustion. SAE International Journal of Engines, 10(4), pp.1491-1505.

[21] Benajes, J., Molina, S., García, A., Belarte, E. and Vanvolsem, M., 2014. An investigation on RCCI combustion in a heavy duty diesel engine using in-cylinder blending of diesel and gasoline fuels. Applied Thermal Engineering, 63(1), pp.66-76.

[22] Reitz, R.D. and Duraisamy, G., 2015. Review of high efficiency and clean reactivity controlled compression ignition (RCCI) combustion in internal combustion engines. Progress in Energy and Combustion Science, 46, pp.12-71.

[23] Walker, N.R., Dempsey, A.B., Andrie, M.J. and Reitz, R.D., 2013. Use of low-pressure direct-injection for reactivity controlled compression ignition (RCCI) light-duty engine operation. SAE International Journal of Engines, 6(2), pp.1222-1237.

[24] Gross, C.W. and Reitz, R., 2017. Investigation of Steady-State RCCI Operation in a Light-Duty Multi-Cylinder Engine Using "Dieseline" (No. 2017-01-0761). SAE Technical Paper.

[25] Wang, H., Zhao, X., Tong, L. and Yao, M., 2018. The effects of DI fuel properties on the combustion and emissions characteristics of RCCI combustion. Fuel, 227, pp.457-468.

[26] Tong, L., Wang, H., Zheng, Z., Reitz, R. and Yao, M., 2016. Experimental study of RCCI combustion and load extension in a compression ignition engine fueled with gasoline and PODE. Fuel, 181, pp.878-886.
[27] Dempsey, A.B., Curran, S. and Reitz, R.D., 2015. Characterization of reactivity controlled compression ignition (RCCI) using premixed gasoline and direct-injected gasoline with a cetane improver on a multi-cylinder engine. SAE International Journal of Engines, 8(2), pp.859-877.
[28] Splitter, D., Hanson, R., Kokjohn, S. and Reitz, R.D., 2011. Reactivity controlled compression ignition (RCCI) heavy-duty engine operation at mid-and high-loads with conventional and alternative fuels (No. 2011-01-0363). SAE Technical Paper.
[29] Aroonsrisopon, T., Foster, D.E., Morikawa, T. and Iida, M., 2002. Comparison of HCCI operating ranges for combinations of intake temperature, engine speed and fuel composition (No. 2002-01-1924). SAE Technical Paper.
[30] Dec, J.E. and Sjöberg, M., 2004. Isolating the effects of fuel chemistry on combustion phasing in an HCCI engine and the potential of fuel stratification for ignition control. SAE transactions, pp.239-257.
[31] Shi, L., Cui, Y., Deng, K., Peng, H. and Chen, Y., 2006. Study of low emission homogeneous charge compression ignition (HCCI) engine using combined internal and external exhaust gas recirculation (EGR). Energy, 31(14), pp.2665-2676.
[32] Splitter, D., Wissink, M., Kokjohn, S. and Reitz, R.D., 2012. Effect of compression ratio and piston geometry on RCCI load limits and efficiency (No. 2012-01-0383). SAE Technical Paper.
[33] Chang, J., Güralp, O., Filipi, Z., Assanis, D., Kuo, T.W., Najt, P. and Rask, R., 2004. New heat transfer correlation for an HCCI engine derived from measurements of instantaneous surface heat flux. SAE transactions, pp.1576-1593.
[34] Hanson, R., Kokjohn, S., Splitter, D. and Reitz, R., 2011. Fuel effects on reactivity controlled compression ignition (RCCI) combustion at low load. SAE International Journal of Engines, 4(1), pp.394-411.
[35] Li, Y., Jia, M., Chang, Y., Xu, Z., Xu, G., Liu, H. and Wang, T., 2018. Principle of determining the optimal operating parameters based on fuel properties and initial conditions for RCCI engines. Fuel, 216, pp.284-295.
[36] Martin, J., Boehman, A., Topkar, R., Chopra, S., Subramaniam, U. and Chen, H., 2018. Intermediate combustion modes between conventional diesel and RCCI. SAE International Journal of Engines, 11(2018-01-0249), pp.835-860.
[37] Sjöberg, M. and Dec, J.E., 2007. EGR and intake boost for managing HCCI low-temperature heat release over wide ranges of engine speed (No. 2007-01-0051). SAE Technical Paper.
[38] Yao, M., Zhang, B., Zheng, Z., Cheng, Z. and Xing, Y., 2005. Experimental Study on the effects of EGR and Octane Number of PRF Fuel on Combustion and Emission Characteristics of HCCI Engines (No. 2005-01-0174). SAE Technical Paper.
[39] Abd-Alla GH. Using exhaust gas recirculation in internal combustion engines: a review. Energy Conversion and Management. 2002 May 1;43(8):1027-42.

Appendix

Table 5: RESULTS FOR PRF50.

PRF	EGR [%]	SOI [ATDC]	Efficiencies [%]		IMEPg [bar]	CA50 [ATDC]	Burn Duration [CAD]	Phi Prime	Emissions [%]			Blend Ratio
			η_comb	η_th_ig					UHC	CO	NOX	
50	30	-65	94.81	36.34	3.57	-4.7	12.1	0.3167	0.2691	0.1428	0.0002	0.77
	35	-45	95.23	35.60	3.60	-4	11.1	0.3272	0.2702	0.1660	0.0006	0.76
		-50	95.22	35.28	3.56	-3.6	11.6	0.3280	0.2714	0.1632	0.0004	0.77
		-55	95.14	36.17	3.64	-3.6	11.6	0.3282	0.2782	0.1592	0.0003	0.78
		-60	94.98	35.92	3.59	-3.4	11.7	0.3257	0.2873	0.1604	0.0002	0.78
		-65	94.87	35.66	3.56	-3.2	12.3	0.3274	0.2913	0.1639	0.0002	0.78
	40	-45	95.18	36.62	3.69	-3.1	11.4	0.3332	0.2903	0.1974	0.0005	0.77
		-50	95.23	36.73	3.70	-2.7	11.6	0.3341	0.2921	0.1886	0.0003	0.77
		-55	94.99	36.42	3.62	-2.5	11.8	0.3304	0.3045	0.1932	0.0003	0.77
		-60	94.91	35.94	3.57	-2.3	12.3	0.3303	0.3059	0.1965	0.0002	0.76
		-65	94.94	36.00	3.57	-2.1	12.7	0.3314	0.3052	0.1964	0.0002	0.76
	45	-45	95.10	36.04	3.71	-1.4	13	0.3420	0.3241	0.2338	0.0003	0.78
		-50	95.12	36.48	3.74	-1.1	12.7	0.3397	0.3307	0.2219	0.0002	0.77
		-55	95.06	36.14	3.69	-0.8	13.4	0.3392	0.3290	0.2268	0.0002	0.77
		-60	94.99	36.63	3.72	-0.7	13.6	0.3398	0.3381	0.2248	0.0001	0.78
		-65	94.95	36.76	3.72	-0.6	13.6	0.3356	0.3379	0.2246	0.0001	0.78
	50	-45	94.52	37.36	3.82	1	15.4	0.3345	0.3610	0.3481	0.0003	0.78
		-50	94.59	37.32	3.79	1	14.8	0.3318	0.3629	0.3212	0.0002	0.78
		-55	94.47	37.59	3.78	1	14.8	0.3295	0.3694	0.3199	0.0002	0.77
		-60	94.45	37.81	3.79	1.2	14.9	0.3299	0.3738	0.3162	0.0002	0.76
		-65	94.43	37.61	3.77	1.1	15.3	0.3322	0.3743	0.3126	0.0002	0.79
	55	-45	93.85	36.63	3.78	3.3	15.9	0.3423	0.4554	0.4349	0.0002	0.78
		-50	93.73	36.83	3.78	3.7	16.5	0.3415	0.4601	0.4456	0.0001	0.78
		-55	93.48	36.89	3.76	4.3	16.9	0.3454	0.4776	0.4641	0.0001	0.78
		-60	93.19	36.77	3.72	4.8	17.6	0.3452	0.4959	0.4866	0.0001	0.80
		-65	93.01	36.92	3.70	4.8	17.7	0.3429	0.5007	0.5025	0.0001	0.78

Table 6: RESULTS FOR PRF60.

PRF	EGR [%]	SOI [ATDC]	Efficiencies [%]		IMEPg [bar]	CA50 [ATDC]	Burn Duration [CAD]	Phi Prime	Emissions [%]			Blend Ratio
			η_comb	η_th_ig					UHC	CO	NOX	
60	25	-45	94.24	36.57	3.66	-4.1	10.4	0.3342	0.2995	0.1482	0.0009	0.77
		-50	94.18	36.78	3.64	-3.5	9.9	0.3286	0.2993	0.1479	0.0006	0.75
		-55	94.08	37.06	3.63	-3.2	10.6	0.3257	0.2998	0.1510	0.0004	0.77
		-60	93.88	37.16	3.60	-2.9	10.9	0.3240	0.3075	0.1544	0.0003	0.75
		-65	93.82	37.28	3.61	-2.8	11.1	0.3244	0.3098	0.1557	0.0003	0.77
	30	-45	94.28	36.99	3.66	-3.1	10.7	0.3288	0.3037	0.1677	0.0006	0.78
		-50	94.29	37.02	3.64	-2.7	11	0.3274	0.3028	0.1654	0.0004	0.77
		-55	94.27	37.06	3.63	-2.4	11.1	0.3256	0.3024	0.1661	0.0003	0.78
		-60	94.16	37.64	3.66	-2.1	11.3	0.3230	0.3040	0.1715	0.0003	0.78
		-65	94.05	37.98	3.67	-1.9	11.9	0.3233	0.3079	0.1758	0.0002	0.76
	35	-45	94.38	37.76	3.60	-2.2	10.1	0.3211	0.3095	0.2091	0.0005	0.76
		-50	94.42	37.78	3.59	-1.8	10.7	0.3210	0.3078	0.2038	0.0003	0.77
		-55	94.22	38.30	3.60	-1.4	10.7	0.3171	0.3164	0.2081	0.0003	0.76
		-60	94.09	38.18	3.57	-1.1	11.4	0.3157	0.3208	0.2116	0.0002	0.78
		-65	93.87	38.18	3.64	-0.8	11.6	0.3138	0.3288	0.2205	0.0002	0.78
	40	-45	94.27	38.08	3.64	-0.5	10.5	0.3225	0.3342	0.2553	0.0003	0.75
		-50	94.19	38.85	3.69	-0.1	11.2	0.3225	0.3384	0.2504	0.0003	0.76
		-55	94.03	39.03	3.68	0.4	11.9	0.3209	0.3445	0.2586	0.0002	0.76
		-60	93.86	38.97	3.64	0.6	11.7	0.3170	0.3506	0.2665	0.0002	0.76
		-65	93.62	38.92	3.63	0.9	12.1	0.3167	0.3606	0.2796	0.0002	0.76
	45	-45	93.65	39.29	3.75	1.4	11.8	0.3250	0.3934	0.3255	0.0003	0.76
		-50	93.67	39.39	3.75	1.8	12.3	0.3253	0.3937	0.3221	0.0002	0.75
		-55	93.47	39.42	3.73	2.2	12.7	0.3235	0.4025	0.3350	0.0002	0.75
		-60	93.28	40.11	3.77	2.5	13.5	0.3230	0.4092	0.3479	0.0002	0.75
		-65	93.00	40.96	3.81	2.7	13.3	0.3220	0.4238	0.3625	0.0002	0.75
	50	-45	92.59	39.96	3.78	3.8	13.9	0.3306	0.4905	0.4427	0.0002	0.77
		-50	92.42	40.19	3.79	4.4	14.5	0.3286	0.4963	0.4645	0.0002	0.77
		-55	92.07	40.11	3.74	4.8	14.8	0.3266	0.5145	0.4841	0.0002	0.77
		-60	91.66	40.25	3.71	5.2	15.4	0.3244	0.5324	0.5159	0.0002	0.77
		-65	91.36	39.91	3.66	5.4	15.9	0.3230	0.5441	0.5386	0.0002	0.76

Table 7: RESULTS FOR PRF70.

PRF	EGR [%]	SOI [ATDC]	Efficiencies [%]		IMEPg [bar]	CA50 [ATDC]	Burn Duration [CAD]	Phi Prime	Emissions [%]			Blend Ratio
			η_comb	η_th_ig					UHC	CO	NOX	
70	0	-45	92.73	36.95	3.50	-4.2	9.3	0.3165	0.2614	0.1490	0.0007	0.76
		-50	92.77	37.61	3.52	-3.7	8.9	0.3121	0.2614	0.1417	0.0004	0.75
		-55	92.70	37.96	3.55	-3.4	9.5	0.3135	0.2639	0.1419	0.0003	0.78
		-60	92.47	38.29	3.55	-3	10.1	0.3115	0.2688	0.1470	0.0002	0.79
		-65	92.24	38.72	3.56	-2.7	9.8	0.3078	0.2762	0.1506	0.0002	0.75
	10	-45	92.76	38.19	3.53	-3.1	10	0.3116	0.2789	0.1796	0.0004	0.75
		-50	92.66	38.45	3.52	-2.6	10.3	0.3091	0.2805	0.1817	0.0003	0.76
		-55	92.53	38.70	3.52	-2.2	10.7	0.3069	0.2835	0.1833	0.0002	0.75
		-60	92.44	39.07	3.54	-1.8	11.2	0.3067	0.2865	0.1832	0.0002	0.76
		-65	92.18	39.18	3.52	-1.5	11.1	0.3039	0.2943	0.1895	0.0001	0.77
	15	-45	93.09	38.40	3.56	-2.7	9.6	0.3124	0.2845	0.1915	0.0004	0.77
		-50	93.02	38.29	3.55	-2.1	10.1	0.3125	0.2867	0.1911	0.0003	0.77
		-55	92.75	38.27	3.52	-1.6	10.3	0.3102	0.2958	0.1971	0.0002	0.75
		-60	92.65	38.63	3.53	-1.2	10.9	0.3089	0.2973	0.1995	0.0002	0.77
		-65	92.51	38.85	3.53	-0.9	11.3	0.3081	0.3019	0.2035	0.0001	0.77
	20	-45	93.11	39.39	3.66	-1.9	10	0.3143	0.2988	0.2061	0.0004	0.75
		-50	93.11	39.77	3.68	-1.3	10.2	0.3119	0.2983	0.2037	0.0002	0.76
		-55	92.94	39.87	3.68	-0.8	10.6	0.3114	0.3046	0.2068	0.0002	0.77
		-60	92.71	40.21	3.68	-0.4	11.1	0.3097	0.3114	0.2150	0.0001	0.76
		-65	92.65	40.43	3.69	-0.2	10.9	0.3080	0.3137	0.2177	0.0001	0.76
	25	-45	93.21	39.39	3.71	-1.2	10.2	0.3163	0.3130	0.2228	0.0003	0.75
		-50	92.92	39.46	3.65	-0.5	11	0.3125	0.3195	0.2322	0.0002	0.76
		-55	92.68	39.67	3.64	0	11.7	0.3113	0.3253	0.2414	0.0002	0.75
		-60	92.37	39.77	3.61	0.5	11.9	0.3075	0.3327	0.2554	0.0001	0.76
		-65	92.02	39.72	3.57	1	12.1	0.3046	0.3417	0.2741	0.0001	0.75
	30	-45	92.83	39.65	3.68	-0.1	10.9	0.3128	0.3374	0.2682	0.0002	0.76
		-50	92.68	39.75	3.66	0.5	11.2	0.3097	0.3409	0.2744	0.0002	0.75
		-55	92.53	39.31	3.60	1	12.3	0.3096	0.3458	0.2798	0.0001	0.77
		-60	92.10	39.50	3.57	1.6	12.2	0.3052	0.3559	0.3046	0.0001	0.76
		-65	91.75	39.82	3.56	2	13	0.3046	0.3656	0.3252	0.0001	0.75

Table 8: RESULTS FOR PRF80.

PRF	EGR [%]	SOI [ATDC]	Efficiencies [%]		IMEPg [bar]	CA50 [ATDC]	Burn Duration [CAD]	Phi Prime	Emissions [%]			Blend Ratio
			η_comb	η_th_ig					UHC	CO	NOX	
80	0	-45	91.60	40.50	3.70	-1.6	9	0.3136	0.2961	0.1841	0.0004	0.76
		-50	91.41	40.77	3.70	-0.9	9.1	0.3105	0.3020	0.1849	0.0003	0.76
		-55	91.18	41.22	3.71	-0.3	9.4	0.3090	0.3067	0.1922	0.0002	0.77
		-60	90.98	41.27	3.69	0.2	9.6	0.3073	0.3126	0.1958	0.0002	0.75
		-65	90.70	41.54	3.69	0.6	9.7	0.3011	0.3191	0.2044	0.0001	0.75
	5	-45	91.46	40.07	3.74	-0.8	10.8	0.3188	0.3157	0.2015	0.0004	0.76
		-50	91.29	40.43	3.76	-0.1	11.2	0.3167	0.3196	0.2052	0.0003	0.77
		-55	90.90	40.63	3.72	0.6	11.3	0.3127	0.3282	0.2174	0.0002	0.78
		-60	90.76	40.85	3.73	1.1	11.6	0.3129	0.3306	0.2224	0.0002	0.77
		-65	90.38	40.98	3.70	1.5	11.8	0.3103	0.3379	0.2379	0.0001	0.75
	10	-45	91.49	39.80	3.72	-0.2	10.6	0.3172	0.3277	0.2244	0.0004	0.76
		-50	91.35	40.17	3.74	0.5	10.8	0.3178	0.3323	0.2271	0.0002	0.77
		-55	91.08	40.06	3.70	1.3	11.4	0.3162	0.3375	0.2377	0.0002	0.77
		-60	90.61	41.41	3.77	2	12.2	0.3123	0.3476	0.2565	0.0002	0.76
		-65	90.26	41.07	3.72	2.4	12.6	0.3123	0.3568	0.2703	0.0001	0.78
	15	-45	91.30	40.98	3.84	0.7	12	0.3203	0.3473	0.2491	0.0003	0.80
		-50	91.21	41.46	3.84	1.7	12.3	0.3179	0.3523	0.2634	0.0002	0.76
		-55	90.75	41.73	3.83	2.4	12.9	0.3162	0.3646	0.2819	0.0001	0.77
		-60	90.47	42.29	3.86	2.9	13.7	0.3161	0.3713	0.2940	0.0001	0.77
		-65	89.93	42.55	3.84	3.5	14.1	0.3151	0.3844	0.3203	0.0001	0.77
	20	-45	91.03	42.42	3.94	1.9	12.5	0.3177	0.3767	0.2944	0.0002	0.77
		-50	90.84	42.27	3.90	2.8	12.9	0.3175	0.3776	0.3106	0.0002	0.77
		-55	90.35	42.28	3.86	3.6	13.5	0.3156	0.3894	0.3350	0.0001	0.77
		-60	89.92	42.66	3.86	4.1	13.6	0.3142	0.4019	0.3556	0.0001	0.77
		-65	89.00	42.63	3.79	4.9	15.1	0.3117	0.4268	0.3998	0.0001	0.77
	25	-45	91.00	42.55	3.95	2.9	13.1	0.3184	0.3976	0.3205	0.0002	0.77
		-50	90.46	42.85	3.92	4	14.1	0.3166	0.4080	0.3554	0.0001	0.78
		-55	89.72	43.04	3.89	4.9	15	0.3144	0.4268	0.3955	0.0001	0.79
	30	-45	90.28	42.85	3.95	4.2	13.6	0.3181	0.4454	0.3779	0.0002	0.77
		-50	89.56	42.30	3.84	5.4	14.6	0.3150	0.4608	0.4267	0.0001	0.77

Table 9: RESULTS FOR PRF90.

PRF	EGR [%]	SOI [ATDC]	Efficiencies [%]		IMEPg [bar]	CA50 [ATDC]	Burn Duration [CAD]	Phi Prime	Emissions [%]			Blend Ratio
			η_comb	η_th_ig					UHC	CO	NOX	
90	0	-45	90.30	40.83	3.77	2.9	11.6	0.3243	0.3487	0.2307	0.0005	0.65
		-50	88.94	41.78	3.74	4.6	12.9	0.3179	0.3832	0.2751	0.0003	0.56
		-55	87.05	41.75	3.64	6.2	15	0.3165	0.4259	0.3501	0.0003	0.66